Frequency-resolved intramolecular excimer fluorescence study of lipid bilayer and nonbilayer phases

Lin-I Liu,* Kwan Hon Cheng,* and Pentti Somerharju‡

*Department of Physics, Texas Tech University, Lubbock, Texas 79409 USA; and ‡Department of Medical Chemistry, University of Helsinki, Siltavuorenpenger 10, 00170 Helsinki, Finland

ABSTRACT Frequency-domain fluorescence intensity decays of the intramolecular excimer forming (DipyPE) in a fully hydrated dioleoylphosphatidylethanolamine (DOPE) suspension have been measured at the monomer (395 nm) and excimer (475 nm) emissions and at different temperatures (0–30°C). A classical Birks (two-state) and a new three-state kinetics models were used to analyze the frequency-domain data. The three-state model allowed us to resolve various intramolecular dynamics parameters of DipyPE in the host DOPE suspension. Those parameters are the excimer association (K_{dm}) and dissociation (K_{md}) rate constants, effective concentration (C), and lateral diffusion rate (f) of the pyrene moieties in the DipyPE. In contrast, only CK_{dm} and K_{md} were determined based on the two-state model. We observed that K_{dm} declined while C increased abruptly at ~12°C, the known thermotropic lamellar liquid crystalline-to-inverted hexagonal (L_α–H_{II}) phase transition temperature of DOPE. No abrupt changes in K_{md} and f were observed at all temperatures. We concluded that the rotation of the lipid acyl chains is hindered and the free volume available for the lipid terminal methyl ends is reduced as the lipid membrane enters the highly curved H_{II} phase from the planar L_α phase.

INTRODUCTION

Several biologically significant lipids, e.g., unsaturated phosphatidylethanolamine (PE), form nonbilayer phases of different packing geometries spontaneously in an aqueous solution upon their isolation from cell membranes (1). At present, the molecular mechanisms that these nonbilayer phase-preferring lipids use to regulate cell membrane activities are still speculative (1–8).

The inverted hexagonal (H_{II}) phase is the most commonly investigated lipid nonbilayer phase. In this H_{II} phase, the lipids form hexagonally packed long water-cored cylindrical tubes in which the lipid polar headgroups are facing the long symmetrical axes of the cylinders. Although the structure and morphologies of this H_{II} phase have been investigated extensively by the x-ray (7–9) and electron microscopic (1) techniques, the detailed molecular dynamics of the lipids in the H_{II} phase, particularly within the nanosecond (or fluorescence) time regime, has become a subject of interest only recently (2–6, 10–12). It is believed that knowledge of both the structure and molecular dynamics of the lipids in the H_{II} phase is required in order to better understand the role of nonbilayer-preferring lipids in the cell membrane function at the molecular level (2).

During the past few years, several nanosecond-resolved fluorescence spectroscopic studies aiming at the understanding of the intermolecular interactions among the lipids in the H_{II} phase have been initiated. These studies involved mainly frequency-domain measurements of the fluorescence anisotropy decays of diphenylhexatriene-labeled phosphatidylcholine (DPH-PC) in several fully hydrated lipid suspensions of PE (2) or mixtures containing PE (2, 12). By the use of different rotational diffusion models, the value of the local orientational order parameter of DPH-PC was found to increase significantly at the temperature- or composition-driven lamellar liquid crystalline (L_α) to H_{II} phase transition of those PE suspensions. On the basis of this observation, it was predicted that the average lateral stress of the lipid layer in the H_{II} phase is higher than that in the L_α phase. At present, the detailed intramolecular dynamics, e.g., acyl chain rotation and intralipid free volume, of the lipids in either the H_{II} or L_α phase have not been fully explored either theoretically or experimentally (6, 13, 14).

In this study, we attempted to investigate the intramolecular dynamics of the lipid acyl chains in both the L_α and H_{II} phases by measuring the excimer formation kinetics of a dual-chain pyrene-labeled lipid embedded in a PE suspension. A fully hydrated dioleoyl PE (DOPE) suspension was used as our lipid membrane system. This DOPE suspension has a well known L_α–H_{II} phase transition at ~10°C (2, 7). At a sufficiently low concentration of dipyrenyl lipids in the host lipid suspension, the measured excimer formation kinetics among the pyrene moieties is solely an intramolecular diffusion-controlled event within a single dipyrenyl lipid (6, 14). In addition, the intermolecular excimer formation between two different dipyrenyl lipids can be ignored (6, 13, 14).

As an intramolecular event, the physical parameters (rotation, lateral diffusion, and free volume) of the two lipid acyl chains within a single dipyrenyl lipid should influence the efficiency of the intramolecular excimer fluorescence of the two pyrene moieties of the dipyrenyl lipid. The classical two-state or Birks model (15), also known as the excited state reaction model, has been used extensively to examine the excimer formation kinetics of molecules in isotropic solutions. However, this two-state model has been shown to be insufficient to delineate the above physical parameters of dipyrenyl lipid in a highly hindered and anisotropic lipid membrane system (6, 13,

Address correspondence to K. H. Cheng at Biophysics Laboratory, Department of Physics, Box 41051, Lubbock, TX 79409-1051.

0006-3495/93/06/1869/09 $2.00

16–18). By using a three-state kinetics model (18), this study attempted to resolve the intralipid dynamic and structural parameters of the lipid acyl chains from the measured monomer and excimer fluorescence decays of the dipyrenyl lipid in the DOPE suspension. The above-mentioned three-state kinetics model was originally used to investigate the intermolecular excimer formation kinetics of the monopyrene-labeled lipids in a lipid bilayer membrane (18). Here we have further extended the application of this three-state model into exploring the intramolecular excimer formation kinetics of the dipyrenyl lipid in a lipid membrane that exhibits both bilayer and nonbilayer phases. A brief description of the two- and three-state models and their major assumptions used in this study is also presented in this paper.

MATERIALS AND METHODS

Sample preparation

DOPE in chloroform was purchased from Avanti Polar Lipids (Birmingham, AL) and used without further purification. No detectable fluorescence signal was found in the pure DOPE suspension. 1-palmitoyl, 2-(1′-pyrene-myristoyl)PE (PyPE), and Di(1′-pyrene-myristoyl)-PE (DipyPE) were synthesized by methods described previously (13, 19). Here PyPE consists of a planar pyrene molecule attached to one terminal methyl end of an acyl chain (*sn-2*) of a PE lipid, and DipyPE has two pyrene molecules separately attached to both terminal methyl ends of the acyl chains (*sn-1* and *sn-2*) of a PE lipid.

Binary PyPE/DOPE and DipyPE/DOPE mixtures were formed in chloroform at the molar ratios of 0.05 and 0.1%, respectively. These lipid mixtures were first dried under nitrogen gas and then kept under vacuum for >5 h to ensure complete removal of chloroform. The dry lipid films were subsequently hydrated in an aqueous buffer (100 mM NaCl/10 mM TES/2 mM EDTA; pH 7.4) at 0°C under mild sonication for a few seconds. Thereafter, the lipid suspensions were incubated at 0°C for ~20 h in the dark to ensure proper hydration of the lipids. After we further diluted the lipid suspensions to 50 μg/ml, each sample was then put into a 10-mm quartz cuvette. During the fluorescence measurement, the sample temperature was regulated by an external water-jet circulator and determined by inserting a microtip thermistor probe (model YSI-427; Yellow Springs Instrument Co., Yellow Springs, OH) into the cuvette at ~5 mm above the light path.

Frequency-domain fluorescence intensity decay measurements

All frequency-domain fluorescence intensity decay measurements were performed on a multifrequency cross-correlation fluorometer (model GREG-200; ISS Inc., Champaign, IL) using a He–Cd laser (model 4240NB; Liconix, Sunnyvale-Santa Clara, CA) with an output of 17 mW at 325 nm as the excitation source. The operational principle of this fluorometer has been described in details elsewhere (20, 21). Since the light exiting from the pockels cell (electro-optical device) is vertically polarized, a polarizer with its polarization axis set at 35° with respect to the vertical was placed in the excitation beam in order to eliminate the contribution of the rotational diffusion effect of the sample to the measurements (2–4, 22, 23).

For the sample containing DipyPE, fluorescence signals at 395 and 475 nm, which correspond to the fluorescence intensity peaks of the monomer and excimer emissions of DipyPE, respectively, were measured through a monochromator (slit width = 2.0 nm). Both the phase delays ($\delta_F - \delta_S$) and demodulation ratios (M_F/M_S) of the fluorescence signal from each sample as compared with that from a standard solution (1,4-bis[2-(5-phenyl-oxazolyl)]]benzene (POPOP) in ethanol, lifetime = 1.34 ns) were measured at different modulation frequencies ranging from 100 kHz to 5 MHz. Here δ_F and δ_S are the phase delay of the signal from the fluorescent sample and that from the reference sample, respectively, and M_F and M_S the intensity modulation values of the fluorescent sample and that of the reference, respectively. For the sample containing PyPE, only the fluorescence signal from the monomer emission (395 nm) was detected. Similar phase delays and demodulation ratios were measured at the same modulation frequencies (100 kHz to 5 MHz). The phase delays and demodulation ratios of DipyPE and PyPE in DOPE as a function of modulation frequency at different temperatures (0–30°C) therefore constitute the frequency-domain fluorescence intensity decay data of this study.

The method of calculating the single fluorescence lifetime of PyPE from the frequency-domain data has been described previously (6). The following sections outline the mathematical models used for calculating the kinetics and physical parameters of DipyPE from the frequency-domain data.

General mathematical models for analyzing the kinetics of pyrene derivatives in a lipid membrane system

Upon excitation by an extremely short (delta) light pulse, the fluorescent states of the pyrene derivatives in a lipid membrane system can be characterized by a state vector $\mathbf{X} = (X_1, X_2, \ldots, X_n)$. Here X_i is defined as the proportion of the excited pyrene derivatives in the ith excited state and n is the total number of excited states (16). The time-dependent fluorescence emission $f(t, \lambda)$ of the pyrene derivatives immediately after the delta excitation at time t and at a particular emission wavelength λ can be expressed as

$$f(t, \lambda) = \sum_{j=1}^{n} S_j(\lambda) X_j(t), \tag{1}$$

where $S_j(\lambda)$ is defined as the species-associated spectrum of the jth excited species (24). The function $f(t, \lambda)$ is also denoted as the delta response function. Assume that the rates of the fluorescence decay processes of those excited pyrene derivatives can be described by a set of first-order linear differential equations (25) of the form

$$dX_i/dt = \sum_{j=1}^{n} T_{ij} X_j, \tag{2}$$

where $\mathbf{T} = \{T_{ij}\}$ is defined as the transfer matrix. The transfer matrix elements T_{ij} depend on the kinetic parameters of the decay processes. In principle, $\mathbf{X}$ can be solved from Eq. 2 upon knowing the appropriate initial conditions of the pyrene derivatives. Once $\mathbf{X}$ is known, the theoretical form of $f(t, \lambda)$ can therefore be determined from Eq. 1.

For the case of frequency-domain measurements, the excitation light is in the form of a sinusoidally modulated function given by $1 + m_x \exp(i\omega t)$, where the m_x and ω are the modulation level and the angular modulation frequency of the excitation light, respectively. The fluorescence emission $F(t, \lambda)$ of the pyrene derivatives due to the sinusoidally modulated excitation is related to the delta response function $f(t, \lambda)$ and is given by

$$\begin{aligned} F(t, \lambda) &= \int_{-\infty}^{t} f(t - t', \lambda)[1 + m_x \exp(i\omega t')]\, dt' \\ &= c(\lambda)[1 + m_x m_E(\omega, \lambda) \exp(i\omega t)], \end{aligned} \tag{3}$$

where $c(\lambda)$ is a proportional factor and $m_E(\omega, \lambda)$ is the complex demodulation factor of the fluorescence emission. It has further been shown (16) that $m_E(\omega, \lambda)$ is associated with the Fourier transform of $f(t, \lambda)$, i.e., $\tilde{f}(\omega, \lambda)$, and is given by

$$m_E(\omega, \lambda) = \tilde{f}(\omega, \lambda)/\tilde{f}(0, \lambda). \tag{4}$$

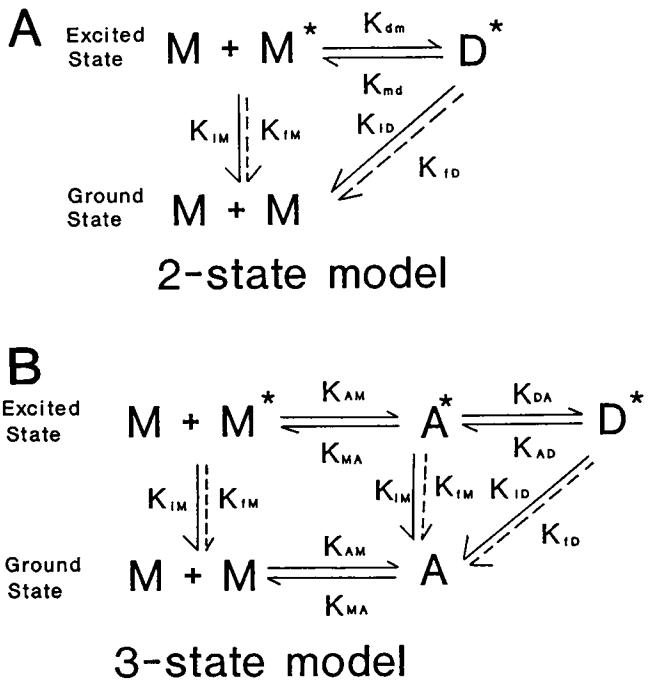

FIGURE 1 Schematic diagrams of the kinetics of excimer formation of pyrene derivatives in a membrane lipid environment based on the two- and three-state kinetics models.

According to Eq. 1, $\tilde{f}(\omega, \lambda)$ is also related with $\tilde{X}_j(\omega)$, the Fourier transform of $X_j(t)$, by the following equation:

$$\tilde{f}(\omega, \lambda) = \sum_{j=1}^{n} S_j(\lambda)\tilde{X}_j(\omega). \quad (5)$$

The absolute value and phase angle of $m_E(\omega, \lambda)$ are equivalent to the demodulation level and phase delay of the fluorescence signal, respectively, as defined in the previous section. In addition, the measurable fluorescence parameter, excimer-to-monomer fluorescence intensity ratio, E/M, is identical to $m_E(0, \lambda_D)/m_E(0, \lambda_M)$, where λ_D and λ_M are the excimer and monomer emission wavelengths, respectively.

Based on a given kinetic model (e.g., two- or three-state model in our case), the explicit form of the transfer matrix T can be constructed. Subsequently, the state vector X, as well as its Fourier transform, can be expressed in terms of the kinetics parameters of the pyrene derivatives (16–18). By measuring either the experimental decay function $f(t, \lambda)$ in the time domain or the demodulation factor $m_E(\omega, \lambda)$ in the frequency domain, the kinetics parameters of the pyrene derivatives can then be calculated from Eq. 2 or 4, respectively, based on a nonlinear least-squares procedure. In the following sections, we summarized the existing kinetic models, two- and three-state, that can be used to calculate the state vector X and its Fourier transform of pyrene derivatives in a lipid membrane system.

Two-state kinetics model

According to the two-state kinetics model, as proposed by Birks (15), there are two excited species of pyrene derivatives, excited monomer M^* and excimer D^*. As shown in the schematic diagram (Fig. 1 *A*), M^* collides with a ground state monomer M and gives rise to D^*, which has a lower electronic energy than M^*. The diffusion-controlled association and dissociation rate constants for the excimer are given by K_{dm} and K_{md}, respectively. The decay behavior of M^* and D^* back to their ground states can be described by several transition rate parameters. Here K_{fm} and K_{im} represent the radiative and nonradiative decay rate constants of M^*, respectively, while K_{fd} and K_{id} represent the radiative and nonradiative decay constants of D^*, respectively.

Within the context of this model, the state vector X is represented by (M^*, D^*), and i = 1 and 2 correspond to the excited monomer and excimer states, respectively. The transfer matrix has the form of

$$T = \begin{bmatrix} -K_{fm} - K_{im} - CK_{dm} & K_{md} \\ CK_{dm} & -K_{fd} - K_{id} - K_{md} \end{bmatrix}, \quad (6)$$

where C is the concentration of the pyrene derivatives in the lipid membrane system. Also the two species-associated spectra $S_j(\lambda)$ for j = 1 and 2 and at the monomer emission wavelength λ_M and excimer emission wavelength λ_D are given by

$$S_1(\lambda_M) = K_{fm}; \quad S_2(\lambda_M) = 0$$
$$S_1(\lambda_D) = 0; \quad S_2(\lambda_D) = K_{fd}. \quad (7)$$

The explicit forms of $\tilde{X}_j(\omega)$, $m_E(\omega, \lambda_M)$, and $m_E(\omega, \lambda_D)$ are shown in the Appendix.

Three-state kinetics model

The three-state kinetics model suggests the existence of three excited species of pyrene derivatives, M^* (i = 1), aggregated state A^* (i = 2), and D^* (i = 3). The new A^* state consists of M^* and M in close apposition. A single rotation of either M^* or M triggers the formation of D^*. A schematic diagram of this three-state model is given in Fig. 1 *B*. Here four rate constants are required in order to describe the formation of D^* from M^*. These constants are the association and dissociation rate constants for the A^* state, i.e., K_{AM} and K_{MA}, respectively, and the association and dissociation rate constants for the D^* state, i.e., K_{DA} and K_{AD}, respectively.

The transfer matrix of this three-state model is given by

$$T = \begin{bmatrix} -K_{fm} - K_{im} - K_{AM} & K_{MA} & 0 \\ K_{AM} & -K_{fm} - K_{im} - K_{MA} - K_{DA} & K_{AD} \\ 0 & K_{DA} & -K_{fd} - K_{id} - K_{AD} \end{bmatrix}. \quad (8)$$

Also the three species-associated spectra $S_j(\lambda)$ for j = 1, 2, and 3 at λ_M and λ_D are given by

$$S_1(\lambda_M) = S_2(\lambda_M) = K_{fm}; \quad S_3(\lambda_M) = 0$$
$$S_1(\lambda_D) = S_2(\lambda_D) = 0; \quad S_3(\lambda_D) = K_{fd}. \quad (9)$$

Now, using a simple two-dimensional lattice model as suggested by Sugar et al. (18), we can visualize the dynamics of excimer formation for pyrene derivatives in a membrane system as a diffusion-controlled process of pyrene moieties in a two-dimensional lattice system. Each lattice point corresponds to one available spatial location for the pyrene moiety to reside in the lipid membrane system. The rate of transition from one lattice point to the other is given by a lateral diffusion-associated rate constant f. The concentration of the pyrene in the lattice system is again given by C. Upon the collision of M^* with M, an A^* state, which consists of two pyrene molecules occupying the two nearest neighboring lattice points, is therefore formed. The transition rate for the A^* state to form a D^* state is given by K_{dm} and the correspond-

ing dissociation rate is given by K_{md}. Note that the K_{dm} and K_{md} in the three-state model are the same as the association and dissociation rate constants for the two-state model, and should be associated with the rotational diffusion rate of the pyrene molecules in the lipid membrane system. The four parameters, f, C, K_{dm}, and K_{md}, as depicted by the above lattice model are related with the rate constants K_{DA}, K_{AD}, K_{AM}, and K_{MA} of the three-state model by the following equations (18):

$$K_{DA} = K_{dm}C/[1 - (1 - C)^6]$$
$$K_{AD} = K_{md}$$
$$K_{AM} = 12fC(1 + C)(C^2 - 3C + 3)$$
$$K_{MA} = 12fC(1 - C)^6(C^2 - C^3 - C + 3)/[1 - (1 - C)^6]. \quad (10)$$

Also the initial values of the state vector $\mathbf{X}$ at $t = 0$ are given by

$$[M^*(0), A^*(0), D^*(0)] = \{RC(1 - C)^6, RC[1 - (1 - C)^6], 0\}, \quad (11)$$

where R is defined as the excited fraction of the probe molecules. Note that the three-state model also predicts that the ground state A can be directly excited to form the excited A state, i.e., A^*. In addition, the rate constants governing the association and dissociation kinetics for the A state are assumed to be equivalent to those for the A^* (18).

The explicit forms of $\tilde{X}_j(\omega)$, $m_E(\omega, \lambda_M)$ and $m_E(\omega, \lambda_D)$ according to this three-state model are shown in the Appendix.

In this study, the pyrene derivative is a dual-chain-labeled DipyPE and the kinetics of the excimer formation among the pyrenes is an intramolecular event. The concentration factor C appearing in both the two- and three-state models is therefore defined as the effective concentration of pyrene in the available lattice space or "free volume" occupied by the terminal methyl ends of a lipid in the membrane system. Here the number of the pyrene moieties in a DipyPE molecule is fixed to two. In the respect, C is inversely proportional to the intralipid free volume of DipyPE at the ends of its hydrocarbon chains.

Data analysis

The intrinsic decay rates ($K_{im} + K_{fm}$) of M^* can be determined independently from the measured fluorescence lifetimes of the mono-labeled pyrene lipid PyPE in the lipid suspension at a very low concentration (PyPE/lipid molar ratio = 0.05%) and at different temperatures. At such a low concentration of PyPE, the intermolecular excimer formation of pyrene moieties in the lipid suspension can be ignored (13). Therefore, the inverses of the values of these lifetimes are then equal to $K_{im} + K_{fm}$.

For the case of the fitting using the two-state model, the unknown parameters in the complex demodulation factor $m_E(\omega, \lambda)$ are CK_{dm}, K_{md}, and ($K_{fd} + K_{id}$) (see Eqs. A1–A4 in the Appendix); whereas for the three-state model, the unknowns are f, C, K_{dm}, K_{md}, K_{fd}/K_{fm}, and ($K_{fd} + K_{id}$) (see Eqs. A5–A9 in the Appendix). The term K_{fd}/K_{fm} is the ratio of the radiative decays of the excimer and monomer. The term ($K_{fd} + K_{id}$) is the intrinsic decay rate of the excimer and was found to be quite insensitive to the physical state of the lipids in both the two- and three-state fits. This parameter was usually fixed in the three-state fit so as to reduce the number of fitting parameters.

A nonlinear least-squares fit procedure using the Marquardt algorithm for minimizing the value of χ^2 was used to determine the unknown physical parameters as described in the two- and three-state models from the frequency-domain data at different wavelengths. For this frequency-domain data analysis, χ^2 is defined as the sum of the square of deviations between the observed and expected phase and modulation values of the fluorescence measurements over all the modulation frequencies. Usually this χ^2 is further divided by the total degrees of freedom of the fitting parameters, in order to obtained the reduced chi-square, χ^2_R. A detailed description of the frequency-domain fitting procedure and the estimation of the confidence limits has been described elsewhere (2, 10, 21).

RESULTS

The values of the phase delay and demodulation level of the fluorescence emissions of DipyPE in DOPE at 395 (monomer) and 475 (excimer) nm were measured as a function of modulation frequency at different temperatures from 0 to 30°C. To calculate the intrinsic rate of monomer decay of pyrene in the lipid membrane, i.e., $K_{im} + K_{fm}$, the fluorescence lifetimes of PyPE in the same DOPE suspension and at identical temperatures were also determined using the frequency-domain tech-

TABLE 1 Comparison of the results from the two- and three-state fits for DipyPE in a fully hydrated DOPE suspension

Fitting parameters	1°C	10°C	25°C
Three-state model			
C	0.72 (0.44, 0.99)	0.29 (0.19, 0.40)	0.69 (0.52, 0.86)
K_{dm} (10^7 s^{-1})	73.5 (57.3, 89.7)	118.6 (72.3, 164.8)	31.9 (18.8, 44.9)
K_{md} (10^7 s^{-1})	7.20 (4.54, 9.86)	2.40 (1.87, 2.93)	2.67 (1.84, 3.50)
f(10^7 s^{-1})	5.90 (3.12, 8.68)	3.51 (2.54, 6.80)	8.30 (4.51, 12.1)
K_{fd}/K_{fm}	0.12 (0.09, 0.15)	0.07 (0.05, 0.09)	0.26 (0.19, 0.33)
χ^2_R	4.45	6.05	2.91
Two-state model			
CK_{dm} (10^7 s^{-1})	56.8 (56.5, 57.1)	84.5 (84.2, 84.8)	31.5 (31.2, 31.8)
K_{md} (10^7 s^{-1})	3.89 (3.57, 4.21)	2.67 (2.35, 2.99)	2.73 (2.49, 2.97)
($K_{fd} + K_{id}$) (10^7 s^{-1})	2.09 (1.64, 2.54)	2.28 (1.81, 2.75)	2.68 (2.34, 3.02)
χ^2_R	64.96	58.77	13.46
($K_{fm} + K_{im}$) (10^7 s^{-1})*	0.66 (0.64, 0.68)	0.78 (0.76, 0.80)	0.91 (0.88, 0.94)

Values in parentheses are confidence limits. DipyPE, dipyrenylphosphatidylethanolamine; DOPE, dioleoylphosphatidylethanolamine; C, effective concentration; K_{dm} and K_{md}, association and dissociation rate constants, respectively; f, lateral diffusion rate; K_{fd} and K_{id}, K_{fm} and K_{im}, radiative and nonradiative decay rate constants for excited D and M states, respectively. * Intrinsic decay rates of pyrene monomer obtained from the fluorescence lifetimes of PyPE in the DOPE suspension.

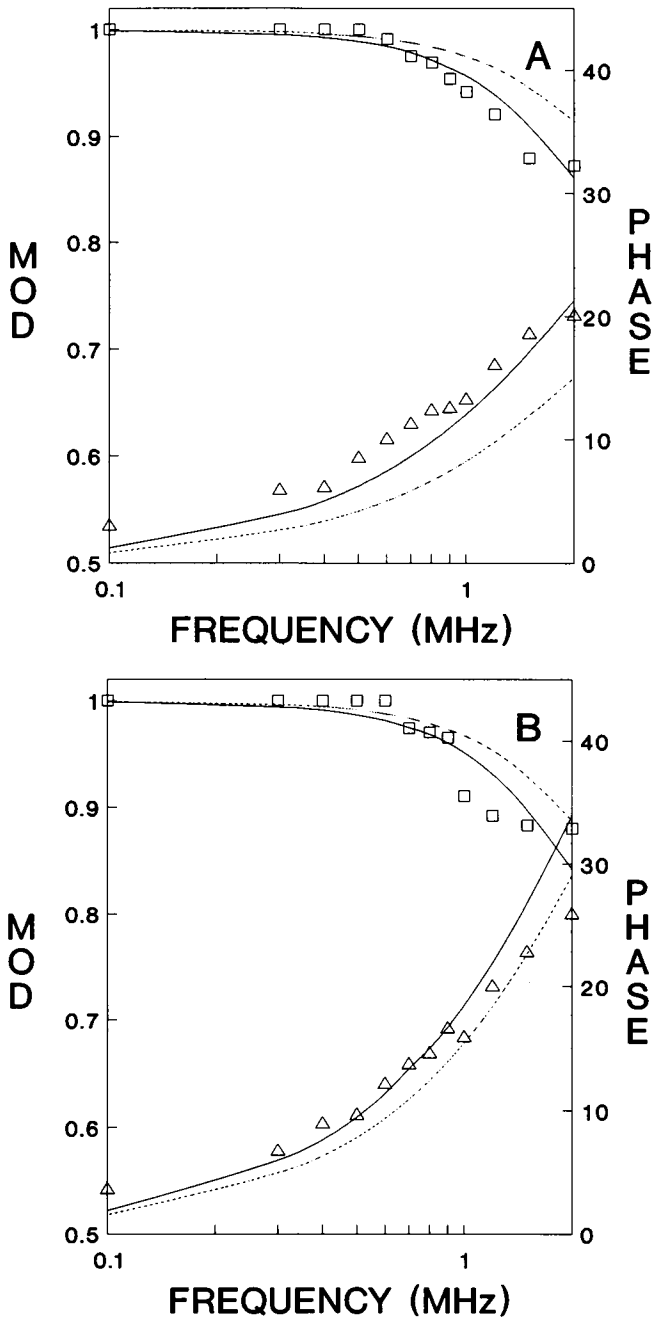

FIGURE 2 Plots of demodulation level (□) and phase delay (△) of the monomer (*A*) and excimer (*B*) fluorescence emissions of DipyPE in a fully hydrated DOPE suspension as a function of modulation frequency of the excitation light at 25°C. The dotted and solid lines represent the theoretical curves generated by the two- and three-state kinetics models, respectively.

nique (see Materials and Methods). The values of $K_{im} + K_{fm}$ increased steadily with temperature.

Both the two- and three-state excimer formation kinetics models were used to analyze the frequency-domain data. For the case of the two-state model, the values of CK_{dm}, K_{md}, and $(K_{fd} + K_{id})$ of DipyPE were determined, while for the case of the three-state model, K_{dm}, K_{md}, f, K_{fd}/K_{fm}, and C of DipyPE were determined. Table 1 shows the typical fitted parameters from both kinetic models at 1, 10, and 25°C. The values of $K_{im} + K_{fm}$ of PyPE are also shown. The values of K_{dm} were found to be >10 times higher than that of K_{md}, while the values of f had the same order magnitude as that of K_{md}. In general, the uncertainties of the fitted parameters from the three-state model were usually higher than those from the two-state model. Yet significant improvements in the values of chi squares from the three-state fit over that from the two-state fit were observed at all temperatures. Fig. 2 shows the typical frequency-domain data and the fitted curves from both models at both the monomer (*A*) and excimer (*B*) emissions at 25°C. It is clear that the three-state model provides a better fit to the frequency-domain data than does the two-state model.

The fitted parameters, CK_{dm}, K_{md}, and $(K_{fd} + K_{id})$, obtained from the two-state model for DipyPE in DOPE as a function of temperature have been determined. For the case of the two-state model, the concentration factor C and K_{dm} cannot be separated. As shown in Fig. 3, the value of CK_{dm} was found to increase progressively with temperature from 0 to 12°C. Thereafter, it dropped abruptly at ~12°C and remained essentially constant as the temperature increased further to 30°C. No similar abrupt changes at ~12°C were found for the other two parameters, K_{md} and $(K_{fd} + K_{id})$ (results not shown).

The fitted parameters, C, K_{dm}, K_{md}, K_{fd}/K_{fm}, and f, obtained from the three-state model for DipyPE in DOPE as a function of temperature have also been determined. Here the C factor and K_{dm} are separately calcu-

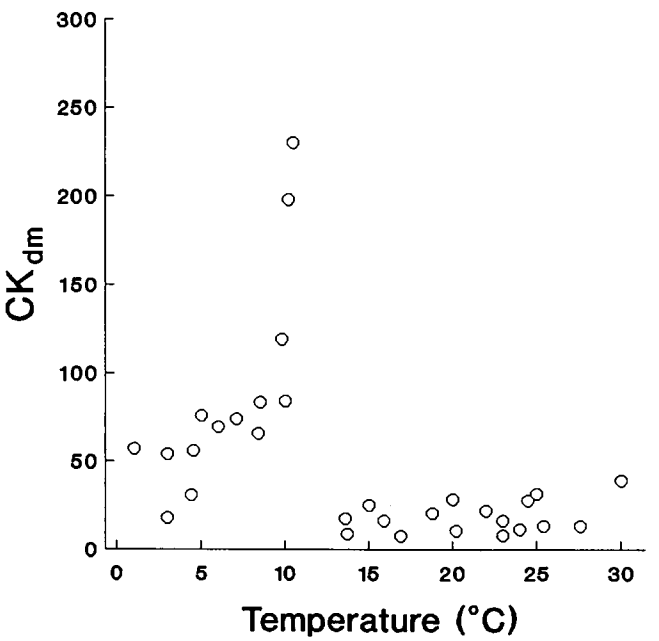

FIGURE 3 A plot of CK_{dm} of DipyPE in a fully hydrated DOPE suspension as a function of temperature. The parameter CK_{dm} was calculated based on a two-state kinetics model. The data points represent results from the fluorescence measurements on three independently prepared samples. The uncertainty is about the same size of the symbol.

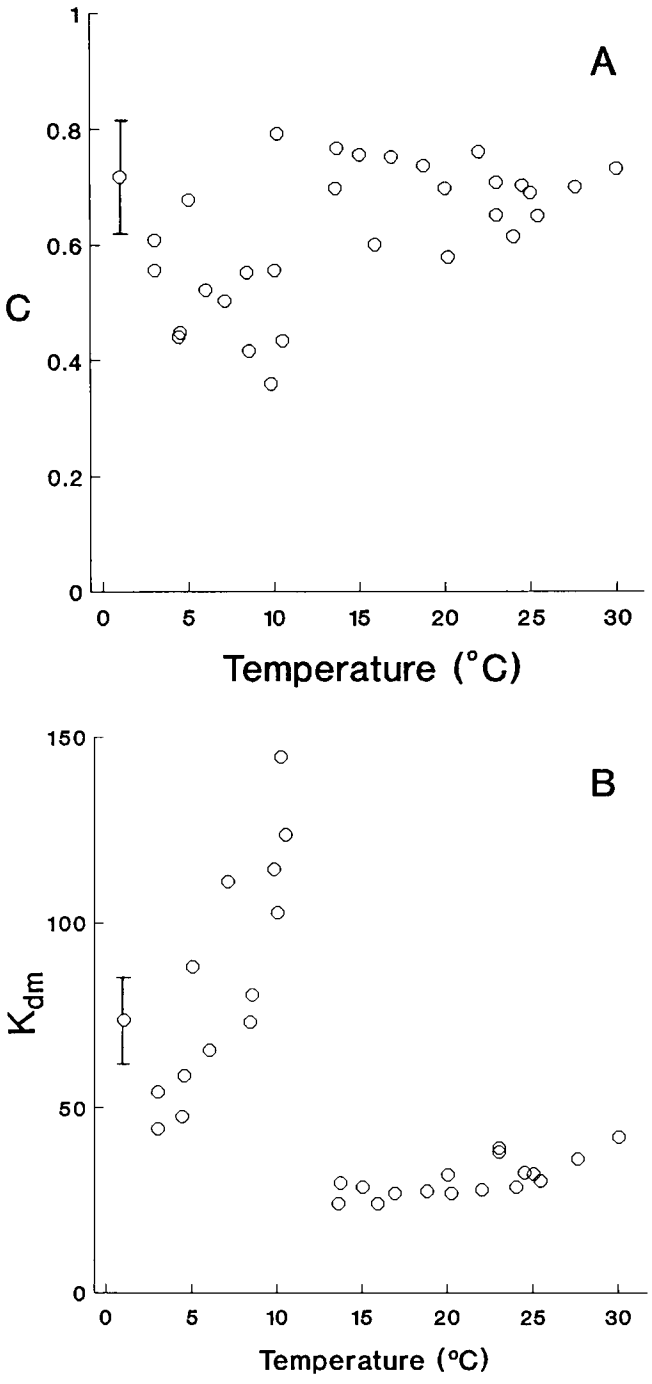

FIGURE 4 Plots of C (A) and K_{dm} (B) of DipyPE in a fully hydrated DOPE suspension as a function of temperature. The parameters were calculated based on the three-state kinetics model. The data points represent results from the fluorescence measurements on three independently prepared samples. The bars indicate the typical uncertainties.

lated, as depicted by the three-state model (see Materials and Methods). As shown in Fig. 4 A, the value of C decreased by ~50% as the temperature was increased from 0 to 12°C. It then increased abruptly at ~12°C and remained high as the temperature was increased to 30°C. Similar to the behavior of CK_{dm} from the two-state model, an abrupt transition, or decrease, in K_{dm} was observed at ~12°C as shown in Fig. 4 B. No changes were found for K_{md}, K_{fd}/K_{fm}, and f at ~12°C (results not shown).

Identical frequency-domain measurements and data analysis for DipyPE in a fully hydrated dioleoylphosphatidylcholine (DOPC) suspension were also performed at identical temperatures (results not shown). No transitions were observed for all the fitted parameters from either the two- or three-state models at all temperatures for DipyPE in DOPC. Since DOPC doesn't exhibit any known phase transition within the temperature range of 0 to 30°C, the changes in the fitted parameters for DipyPE in DOPE at ~12°C are therefore associated specifically to the known L_α–H_{II} phase transition of DOPE at the same temperature range (2, 5, 11).

DISCUSSION

The intramolecular excimer formation kinetics of DipyPE in DOPE have been investigated. On the basis of both the classical two-state and the new three-state models, significant changes in the excimer association rate constant and the effective concentration of the pyrene moieties of DipyPE were detected at the known L_α–H_{II} phase transition of DOPE. As a control, no similar changes in those parameters were detected for DipyPE in DOPC at all temperatures. How do the above observations provide new insights into understanding the intramolecular interactions of the lipid acyl chains in both the L_α and H_{II} phases?

The dynamic parameter K_{dm} is associated with the rotational mobility of the acyl chains in a lipid. The two-state model assumes that the excimer formation is a one-step process in which the two pyrene moieties within the DipyPE diffuse toward each other and form an excimer. The fitted parameter CK_{dm} obtained from this two-state model contains both the geometrical (C) and dynamic (K_{dm}) factors. Therefore, a decrease in CK_{dm} may be due to a decrease in either C or K_{dm} (6). Moreover, as a one-step process, the K_{dm} is influenced by both the lateral and rotational diffusion behavior of the pyrene moieties in the lipid membrane. On the other hand, according to the three-state model, the excimer formation involves an intermediate aggregated state A. The excited A state, i.e., A^*, can be formed from the M and M^* states, or directly from the A state upon excitation. On the basis of a simple two-dimensional lattice model (18), the contributions from the geometry, lateral mobility, and rotational mobility of the pyrene moieties in the lipid membranes are separated and characterized by C, f, and K_{dm}, respectively. Interestingly, the values of CK_{dm} and K_{dm} obtained from the two- and three-state models, respectively, declined abruptly at the L_α–H_{II} transition of DOPE. Therefore we concluded that the rotational mobility of the lipid acyl chains in the H_{II} phase is significantly hindered compared with that in the L_α phase.

The effective concentration C is an interesting geometrical factor used in this study to characterize the free volume available for the pyrene moieties of DipyPE in the lipid membrane system. As discussed in Materials and Methods, C is inversely related to the intramolecular free volume of DipyPE at the ends of the fatty acyl chains where the pyrene molecules are attached. Now, if the ends of the lipid acyl chains are more tightly packed, the number of lattice points available for the pyrene moieties to reside will consequently be decreased. On the basis of the observation that C increased abruptly as the lipid entered the H_{II} phase (Fig. 4 *A*), we concluded that the available lattice space or intralipid free volume available to the terminal ends of the lipid acyl chains in the highly curved H_{II} phase is smaller than that in the planar L_α phase.

How well does the three-state model describe the intramolecular dynamics and free volume of a lipid in the lipid membrane system? It is important to state that the modification of the three-state model originally proposed by Sugar et al. (18) is only the first step in exploring the complicated intramolecular dynamics of lipid acyl chains in a lipid membrane system. The important assumption of using the two-dimensional lattice points to represent the three-dimensional spatial locations of the pyrene moieties of DipyPE in the lipid layer may not be justified. Furthermore, whether the two pyrene moieties in the proposed discrete lattice space are truly randomly distributed is still not known (Sugar, I. P., personal communication). Even with the above uncertainties, this study represents an initial attempt to use a simple model to investigate the intramolecular dynamics of a lipid in the bilayer and nonbilayer phases on the basis of the frequency-domain fluorescence intensity decay measurements of DipyPE. Two thorough studies on the use of dipyrenyl-labeled PC in investigating the temperature and pressure dependence of the intramolecular dynamics of lipids in the lamellar phase have been carried out previously (13, 26). A random walk model was used in these studies to analyse the E/M ratio data of dipyrenyl-labeled PC and monopyrenyl-labeled PC in various PC lipids.

Our present intramolecular dynamics study of DOPE suggests that the intralipid rotational rate and free volume of the acyl chains decrease as the lipids enter the H_{II} phase from the L_α phase. The conclusion obtained from this study appears to complement that from our previous intermolecular dynamics study of DPH-PC (2) as well as the interfacial conformation study of C=O stretching (5) in the identical DOPE suspension. The results of those two previous studies indicated that the average packing of the lipid chains and that of the lipid/water interfacial region in the H_{II} phase are significantly higher than those in the L_α phase. Moreover, the reorientational rate, wobbling diffusion, of DPH-PC is significantly hindered as the DOPE lipids enter the H_{II} phase from the L_α phase. Therefore both the intermolecular and intramolecular interactions among the lipid fatty acyl chains as well as the interfacial conformation at the lipid/water region of the lipids change drastically at the L_α-to-H_{II} transition. Specifically, the packing order and motional constraints of the lipids across the whole hydrocarbon region are significantly higher in the curved H_{II} phase than in the planar L_α phase at the nanosecond (fluorescence) and subpicosecond (infrared absorption) time scales. The question of whether the intramolecular dynamics of the lipids in a lipid bilayer may also be affected by the presence of the nonbilayer phase-preferring lipids is still not answered and will be explored in our future study.

APPENDIX

Solutions of the two-state kinetics model

On the basis of the transfer matrix as given in Eq. 6, the state vector elements $\mathbf{X}_1$ and $\mathbf{X}_2$ in the time space as well as their Fourier transform in the frequency space have been determined (16, 23). The latter are given by

$$\tilde{\mathbf{X}}_1(\omega) = \frac{\begin{bmatrix} -M(0) & K_{md} \\ 0 & -K_{fd} - K_{id} - K_{md} - i\omega \end{bmatrix}}{\begin{bmatrix} -K_{fm} - K_{im} - CK_{dm} - i\omega & K_{md} \\ CK_{dm} & -K_{fd} - K_{id} - K_{md} - i\omega \end{bmatrix}} \tag{A1}$$

$$\tilde{\mathbf{X}}_2(\omega) = \frac{\begin{bmatrix} -K_{fm} - K_{im} - CK_{dm} - i\omega & -M(0) \\ CK_{dm} & 0 \end{bmatrix}}{\begin{bmatrix} -K_{fm} - K_{im} - CK_{dm} - i\omega & K_{md} \\ CK_{dm} & -K_{fd} - K_{id} - K_{md} - i\omega \end{bmatrix}}. \tag{A2}$$

From Eqs. A1, A2, 5, and 7, $\tilde{f}(\omega, \lambda)$ at λ_M and λ_D can be written as

$$\tilde{f}(\omega, \lambda_M) = K_{fm}\tilde{\mathbf{X}}_1(\omega)$$
$$\tilde{f}(\omega, \lambda_D) = K_{fd}\tilde{\mathbf{X}}_2(\omega). \tag{A3}$$

On the basis of Eqs. A3 and 4, $m_E(\omega, \lambda)$ at λ_M and λ_D can be expressed as

$$m_E(\omega, \lambda_M) = \tilde{\mathbf{X}}_1(\omega)/\tilde{\mathbf{X}}_1(0)$$
$$m_E(\omega, \lambda_D) = \tilde{\mathbf{X}}_2(\omega)/\tilde{\mathbf{X}}_2(0). \tag{A4}$$

Solutions of the three-state kinetics model

On the basis of Eqs. 8, 10, and 11, the state vector elements $\mathbf{X}_1$, $\mathbf{X}_2$ and $\mathbf{X}_3$ in the time space as well as their Fourier transforms in the frequency space have been solved. The latter are given in reference 18.

$$\hat{\mathbf{X}}_1(\omega) = \frac{\begin{bmatrix} -M^*(0) & K_{MA} & 0 \\ -A^*(0) & -K_{fm} - K_{im} - K_{MA} - K_{DA} - i\omega & K_{AD} \\ 0 & K_{DA} & -K_{fd} - K_{id} - K_{AD} - i\omega \end{bmatrix}}{\begin{bmatrix} -K_{fm} - K_{im} - K_{AM} - i\omega & K_{MA} & 0 \\ K_{AM} & -K_{fm} - K_{im} - K_{MA} - K_{DA} - i\omega & K_{AD} \\ 0 & K_{DA} & -K_{fd} - K_{id} - K_{AD} - i\omega \end{bmatrix}} \tag{A5}$$

$$\hat{\mathbf{X}}_2(\omega) = \frac{\begin{bmatrix} -K_{fm} - K_{im} - K_{AM} - i\omega & -M^*(0) & 0 \\ -K_{AM} & -A^*(0) & K_{AD} \\ 0 & 0 & -K_{fd} - K_{id} - K_{AD} - i\omega \end{bmatrix}}{\begin{bmatrix} -K_{fm} - K_{im} - K_{AM} - i\omega & K_{MA} & 0 \\ K_{AM} & -K_{fm} - K_{im} - K_{MA} - K_{DA} - i\omega & K_{AD} \\ 0 & K_{DA} & -K_{fd} - K_{id} - K_{AD} - i\omega \end{bmatrix}} \tag{A6}$$

$$\hat{\mathbf{X}}_3(\omega) = \frac{\begin{bmatrix} -K_{fm} - K_{im} - K_{AM} - i\omega & K_{MA} & -M^*(0) \\ -K_{AM} & -K_{fm} - K_{im} - K_{MA} - K_{DA} - i\omega & -A^*(0) \\ 0 & K_{DA} & 0 \end{bmatrix}}{\begin{bmatrix} -K_{fm} - K_{im} - K_{AM} - i\omega & K_{MA} & 0 \\ K_{AM} & -K_{fm} - K_{im} - K_{MA} - K_{DA} - i\omega & K_{AD} \\ 0 & K_{DA} & -K_{fd} - K_{id} - K_{AD} - i\omega \end{bmatrix}} \tag{A7}$$

From Eqs. A5–A7, 5, and 9, $\tilde{f}(\omega, \lambda)$ at λ_M and λ_D can be written as

$$\tilde{f}(\omega, \lambda_M) = K_{fm}[\tilde{\mathbf{X}}_1(\omega) + \tilde{\mathbf{X}}_2(\omega)]$$
$$\tilde{f}(\omega, \lambda_D) = K_{fd}\tilde{\mathbf{X}}_3(\omega). \tag{A8}$$

On the basis of Eqs. A8 and 4, $m_E(\omega, \lambda)$ at λ_M and λ_D can be expressed as

$$m_E(\omega, \lambda_M) = [\tilde{\mathbf{X}}_1(\omega) + \tilde{\mathbf{X}}_2(\omega)]/[\tilde{\mathbf{X}}_1(0) + \tilde{\mathbf{X}}_2(0)]$$
$$m_E(\omega, \lambda_D) = \tilde{\mathbf{X}}_3(\omega)/\tilde{\mathbf{X}}_3(0). \tag{A9}$$

We thank Dr. I. P. Sugar at the Mount Sinai Medical Center and Dr. B. W. Van Der Meer at the University of Western Kentucky for the enlightening discussions of the theoretical aspects of the excited state reaction models in this study.

This work was supported by grant D-1158 from the Robert A. Welch Research Foundation to K. H. Cheng and by a grant from the Finnish Academy to P. Somerharju.

Received for publication 14 August 1992 and in final form 1 February 1993.

REFERENCES

1. Cheng, K. H., and S. W. Hui. 1986. Correlation between the bilayer stabilization and activity enhancement by diacylglycerols in reconstituted Ca-ATPase vesicles. *Arch. Biochem. Biophys.* 244:382–386.
2. Cheng, K. H. 1989. Fluorescence depolarization study of lamellar liquid crystalline to inverted cylindrical micellar phase transition of phosphatidylethanolamine. *Biophys. J.* 55:1025–1031.
3. Cheng, K. H. 1989. Fluorescence depolarization study on non-bilayer phases of phosphatidylethanolamine and phosphatidylcholine lipid mixtures. *Chem. Phys. Lipids.* 51:137–145.
4. Cheng, K. H. 1989. Time-resolved fluorescence depolarization study of lamellar to inverted cylindrical micellar phase. *Proc. SPIE Int. Soc. Opt. Eng.* 1054:160–167.
5. Cheng, K. H. 1991. Infrared study of the polymorphic phase behavior of dioleoylphosphatidylethanolamine and dioleoylphosphatidylcholine. *Chem. Phys. Lipids.* 60:119–125.
6. Cheng, K. H., S.-Y. Chen, P. Butko, B. W. Van Der Meer, and P. Somerharju. 1991. Intramolecular excimer formation of pyrene-labeled lipids in lamellar and inverted hexagonal phases of lipid mixtures containing unsaturated phosphatidylethanolamine. *Biophys. Chem.* 39:137–144.
7. Gawrisch, K., V. A. Parsegian, D. A. Hajduk, M. W. Tate, S. M. Gruner, N. L. Fuller, and R. P. Rand. 1992. Energetics of a hexagonal-lamellar-hexagonal phase transition sequence in dioleoylphosphatidylethanolamine membranes. *Biochemistry.* 31:2856–2864.
8. Seddon, J. M. 1990. Structure of the inverted hexagonal (H_{II}) phase, and non-lamellar transitions of lipids. *Biochim. Biophys. Acta.* 1031:1–69.
9. Rand, R. P., N. L. Fuller, S. M. Gruner, and V. A. Parsegian. 1990. Membrane curvature, lipid segregation, and structural transitions for phospholipids under dual-solvent stress. *Biochemistry.* 29:76–87.
10. Chen, S.-Y., K. H. Cheng, B. W. Van Der Meer, and J. M. Beechem. 1990. Effects of lateral diffusion on the fluorescence anisotropy in hexagonal lipid phase II. An experimental study. *Biophys. J.* 58:1527–1537.
11. Chen, S.-Y., K. H. Cheng, and D. M. Ortalano. 1990. Lateral diffusion study of excimer forming lipids in lamellar to inverted hexagonal phase transition of unsaturated phosphatidylethanolamine. *Chem. Phys. Lipids.* 53:321–330.
12. Chen, S.-Y., K. H. Cheng, and B. W. Van Der Meer. 1992. Quantitation of lateral stress in lipid layer containing nonbilayer phase preferring lipids by frequency-domain fluorescence spectroscopy. *Biochemistry.* 31:3759–3768.
13. Vauhkonen, M., M. Sassaroli, P. Somerharju, and J. Eisinger. 1990. Dipyrenylphosphatidylcholines as membrane fluidity

probes. Relationship between intramolecular and intermolecular excimer formation rates. *Biophys. J.* 57:291–300.

14. Eklund, K. K., J. A. Virtanen, P. K. J. Kinnunen, J. Kasurinen, and P. J. Somerharju. 1992. Conformation of phosphatidylcholine in neat and cholesterol containing crystalline bilayers. Application of a novel method. *Biochemistry.* 31:8560–8565.
15. Birks, J. B., D. J. Dyson, and I. H. Munro. 1963. "Excimer" fluorescence II. Lifetime studies of pyrene solutions. *Proc. R. Soc. Lond.* 275:575–588.
16. Sugar, I. P. 1991. Use of fourier transforms in the analysis of fluorescence data. 1. A general method for finding explicit relationships between photophysical methods and fluorescence parameters. *J. Phys. Chem.* 95:7508–7515.
17. Sugar, I. P., J. Zeng, M. Vauhkonen, P. Somerharju, and P. L.-G. Chong. 1991. Use of Fourier transforms in the analysis of fluorescence data. 2. Fluorescence of pyrene-labeled phosphatidylcholine in lipid bilayer membrane. Test of the Birks model. *J. Phys. Chem.* 95:7516–7523.
18. Sugar, I. P., J. Zeng, and P. L.-G. Chong. 1991. Use of fourier transforms in the analysis of fluorescence data. 3. Fluorescence of pyrene-labeled phosphatidylcholine in lipid bilayer membrane. A three-state model. *J. Phys. Chem.* 95:7524–7534.
19. Patel, K. M., J. D. Morrisett, and J. T. Sparrow. 1979. A convenient synthesis of phosphatidylcholine acylation of *sn*-glycero-3-phosphocholine with fatty acid anhydride and 4-pyrrolidinopyrine. *J. Lipid Res.* 20:674–677.
20. Lakowicz, J. R. 1983. Principles of Fluorescence Spectroscopy. Plenum Publishing Corp., New York. 126 pp.
21. Gratton, E., D. M. Jameson, and R. D. Hall. 1984. Multifrequency phase and modulation fluorometry. *Annu. Rev. Biophys. Bioeng.* 13:105–124.
22. Spencer, R. D., and G. Weber. 1970. Influence of Brownian rotations and energy transfer upon the measurements of fluorescence lifetime. *J. Chem. Phys.* 52:1654–1663.
23. Chong, P. L., and T. E. Thompson. 1985. Oxygen quenching of pyrene–lipid fluorescence in phosphatidylcholine vesicles. A probe for membrane organization. *Biophys. J.* 47:613–621.
24. Davenport, L., J. R. Knutson, and L. Brand. 1986. Excited-state proton transfer of equilenin and dihydroequilenin: interaction with bilayer vesicles. *Biochemistry.* 25:1186–1195.
25. Ameloot, M., J. M. Beechem, and L. Brand. 1986. Compartmental modeling of excited-state reactions: identifiability of the rate constants from fluorescence decay surfaces. *Chem. Phys. Lett.* 129:211–219.
26. Sassaroli, M., M. Vauhkonen, P. Somerharju, and S. Scarlata. 1983. Diphenylphosphatidylcholines as membrane fluidity probe. Pressure and temperature dependence of the intramolecular rate. *Biophys. J.* 64:137–149.